Evaluation of a New Polarimetric Algorithm for Rain-Path Attenuation Correction of X-Band Radar Observations Against Disdrometer

John Kalogiros, Marios N. Anagnostou, Emmanouil N. Anagnostou, Mario Montopoli, Errico Picciotti, and Frank Silvio Marzano, *Senior Member, IEEE*

***Abstract*— A new algorithm called self-consistent with optimal parameterization (SCOP) for attenuation correction of radar reflectivities at low elevation angles is developed and evaluated. The SCOP algorithm, which uses optimal parameterization and best-fitted functions of specific attenuation coefficients and backscattering differential phase shift, is applied to X-band dual-polarization radar data and evaluated on the basis of radar observables calculated from disdrometer data at a distance of 35 km from the radar. The performance of the SCOP algorithm is compared with other algorithms [reflectivity-differential phase shift (ZPHI) and full self-consistent (FSC)] presented in the literature. Overall, the new algorithm performs similarly to ZPHI for the attenuation correction of horizontal-polarization reflectivity, whereas the FSC algorithm exhibits significant underestimation. The ZPHI algorithm tends to overestimate small rain-path attenuation values. All algorithms exhibit significant underestimation at high differential rain-path attenuation values, probably due to the presence of hail along the path of the radar beam during the examined cases. The new SCOP algorithm has the potential to retrieve profiles of horizontal and differential reflectivities with better accuracy than the other algorithms due to the low error of the parameterization functions used in it. Typical radar calibration biases and measurement noise are sufficient requirements to ensure low errors of the proposed algorithm. A real-time method to calibrate the differential reflectivity without additional measurements is also described.**

***Index Terms*— Disdrometer, dual-polarization weather radar, rain-path attenuation, X-band.**

Manuscript received June 25, 2012; revised December 7, 2012; accepted February 20, 2013. Date of publication April 17, 2013; date of current version December 12, 2013. This work was supported in part by the HYDRORAD Project Research for SMEs category – Grant Agreement FP7-SME-2008-1-232156 funded by EC 7th Framework Program from 2009 to 2011. The work of M. N. Anagnostou was supported by the Marie Curie Fellowship under Grant Agreement 236871 HYDREX, coordinated by the Sapienza University of Rome, Italy and the Post-Doctoral Fellowship by the Greek General Secretariat for Research and Technology under Grant Agreement PE10(975) HYDRO-X, coordinated by the National Observatory of Athens, Greece, in the framework of the program "Education and Lifelong Learning" funded by Greece and EU-European Social Fund.

J. Kalogiros is with the Institute of Environmental Research and Sustainable Development, National Observatory of Athens, Athens 15236, Greece (e-mail: jkalog@noa.gr).

M. N. Anagnostou is with the Institute of Environmental Research and Sustainable Development, National Observatory of Athens, Athens 15236, Greece, and also with the Department of Information Engineering, Sapienza University of Rome, Rome 153, Italy (e-mail: ma111@engr.uconn.edu).

E. N. Anagnostou is with the Department of Civil and Environmental Engineering, University of Connecticut, Storrs, CT 06250 USA (e-mail: manos@engr.uconn.edu).

M. Montopoli is with the Department of Geography, University of Cambridge, Cambridge CB23 8AQ, U.K., and also with the CETEMPS Centre of Excellence, University of L'Aquila, L'Aquila 67100, Italy (e-mail: mario.montopoli@gmail.com).

E. Picciotti is with the CETEMPS Centre of Excellence, University of L'Aquila, L'Aquila 67100, Italy (e-mail: errico.picciotti@himet.it).

F. S. Marzano is with the Department of Information Engineering, Sapienza University of Rome, Rome 153, Italy, and also with the CETEMPS Centre of Excellence, University of L'Aquila, L'Aquila 67100, Italy (e-mail: marzano@diet.uniroma1.it).

Digital Object Identifier 10.1109/TGRS.2013.2250979

I. Introduction

TECHNOLOGICAL improvement in dual-polarization weather radars has advanced the quantitative estimation of rainfall rate and raindrop size distribution (DSD) parameters [1]. The main measurements of polarimetric radar include the radar reflectivity (Z_h) at horizontal polarization, the differential reflectivity (Z_{dr}), and the specific differential propagation phase shift (K_{dp}), which is estimated from differential phase shift (Φ_{dp}) measurements. At frequencies higher than S-band (2–4 GHz), the attenuation of radar signal by rain can be quite significant. On the other hand, at such frequencies, and especially at X-band (8–12 GHz), weather radars exhibit some unique advantages including the use of smaller-sized antennas for the same required beamwidth and higher sensitivity of the differential phase shift to rainfall rate.

Many attenuation correction methods, which use polarimetric observations and are based mostly on Φ_{dp} measurements, have been developed in the last decade. Some methods approximate the specific horizontal attenuation in rain (A_h) and the specific differential attenuation (A_{dp}) with a fixed linear dependence on K_{dp} [2] or an average proportionality constant estimated from radar data and additional correction for big drops [3]. Other methods use the total Φ_{dp} as a constraint in the attenuation correction [4], or estimate the proportionality constants of the dependence of A_h and A_{dp} on K_{dp} with constrained self-consistent and more complex schemes applied to separate rain cells [5]–[9] or coupled with hydrometeor classification schemes [10]. In order to reduce the effect of noise in polarimetric measurements and correct for path attenuation, a variational retrieval scheme along the radar ray in combination with a forward model (lookup tables obtained from scattering simulations) of polarimetric observables and a complex spatial smoothing technique is used in [11]. In a similar approach, an extended Kalman filter, instead of the variational scheme of [11], is proposed in [12] with a simplified model of average consistency between the polarimetric observables derived from the disdrometer data of an experimental campaign. A relatively

simple self-consistent iterative scheme was presented by [13] and [14] and applied directly to an entire radar ray instead of separate rain cells. However, it keeps the shape of the range profile of specific attenuation estimates from a previous method [4], changing only the total attenuation in order to minimize the difference between the estimated Φ_{dp} profile and the measured one. Furthermore, its results depend on the accuracy of the parameterization functions A_h and A_{dp} from dual-polarization measurements.

This paper presents and evaluates a new self-consistent iterative scheme for attenuation correction of X-band radar Z_h and Z_{dr} measurements using parameterization functions with minimum parameterization error (optimal) of A_h and A_{dp}. These functions have been developed together with parameterizations for the estimation of rain microphysical parameters and rainfall rate from dual-polarization radar measurements in [15]. In Section II, the new self-consistent with optimal parameterizations (SCOP) algorithm is presented, and in Section III its accuracy is examined using concurrent X-band dual-polarization radar and disdrometer data. Comparison of the performance of the new algorithm against other attenuation-correction methods is also presented. It should be noted that the SCOP attenuation correction scheme can also be applied to other attenuated radar frequencies, such as at C-band (4–8 GHz), after recalibration of the corresponding parameterizations using T-matrix scattering simulations.

II. Attenuation Correction Algorithm

A. Parameterization Functions

The basis of the attenuation correction algorithm is the new parameterizations of A_h and A_{dp} from dual-polarization radar observables Z_h, Z_{dr}, and K_{dp} in rain, which were found from T-matrix scattering simulations at X-band (9.37 GHz), carried out for a very wide range of values of rain DSD and drop shape parameters, air temperature, and an elevation of the radar antenna close to zero [15]. These parameterizations minimize the inherent statistical regression error (maximum error of about 5%) using the theoretical Rayleigh scattering limit corrected by a multiplicative rational polynomial function of reflectivity-weighted raindrop diameter (D_z) to approximate the Mie character of scattering at these electromagnetic frequencies. The reflectivity-weighted mean diameter is given by $D_z = E[D^7]/E[D^6]$ [1], where D is the raindrop spherical-equivolume diameter, and E stands for the expectation value. The expectation value is estimated in practice as the DSD-weighted integral over the whole range of diameter values. The parameterization functions for the estimation of D_z (mm), A_h, (dB km^{-1}), A_{dp} (dB km^{-1}), and the backscattering differential phase shift δ_b (deg), which are used in the attenuation correction scheme, as found in [15], for D_z in the range 0.5–8 mm are

$$D_z = D_{z1}\, f_{D_{z1}}(D_{z1})$$

$$D_{z1} = 0.1802\left[\frac{Z_h}{K_{dp}}\xi_{dr}^{-0.2929}\left(1-\xi_{dr}^{-0.4922}\right)\right]^{1/3} \quad (1a)$$

$$D_z = D_{z2}\, f_{D_{z2}}(D_{z2}), \quad D_{z2} = 2.4780\left(1-\xi_{dr}^{-0.5089}\right) \quad (1b)$$

$$\delta_b = 1.2891\xi_{dr}^{0.3566}\left(1-\xi_{dr}^{-0.7447}\right) f_{\delta_b}(D_z) \quad (2)$$

$$A_h = 3.1482\times10^{-5} Z_h \xi_{dr}^{-0.1368} D_z^{-3} f_{A_{h1}}(D_z) \quad (3a)$$

$$A_h = 6.6888\times10^{-4}\left[K_{dp}\xi_{dr}^{0.3024}/\left(1-\xi_{dr}^{-0.2107}\right)\right] f_{A_{h2}}(D_z) \quad (3b)$$

$$A_{dp} = 3.1646\times10^{-5} Z_h\left(\xi_{dr}^{-0.1991}-\xi_{dr}^{-0.5254}\right) \times D_z^{-3} f_{A_{dp1}}(D_z) \quad (4a)$$

$$A_{dp} = 8.0295\times10^{-4} K_{dp} \times\left[\left(\xi_{dr}^{0.5025}-\xi_{dr}^{-0.5025}\right)/\left(1-\xi_{dr}^{-0.2262}\right)\right]\cdot f_{A_{dp2}}(D_z) \quad (4b)$$

where ξ_{dr} is the differential reflectivity in linear units (ratio of reflectivity at horizontal and vertical polarization) and Z_h in these relations is also given in linear units (mm^6 m^{-3}) instead of the usual logarithmic units (dBZ). The ranges of the main simulation parameters are: $5 \le T \le 20$ °C, $1 \le \log_{10}(N_w) \le 5$ m^{-3} mm^{-1}, $0.5 \le D_z \le 8.0$ mm, $Z_h \le 65$ dBZ, $0.2 \le K_{dp} \le 20$ deg km^{-1}, and $R \le 300$ mm h^{-1}. T is the air temperature in the radar sampling volume, N_w is the intercept parameter of the DSD (assumed to be a normalized Gamma function [1]), and R is the rainfall rate. Equation (1b) is valid only for the equilibrium value (equal to 0.066 mm^{-1}) of the effective slope parameter (β_e) of the raindrop axis ratio against drop diameter and should be used only in case of missing or very low (and close to noise) K_{dp} measurements. Note that (3b) and (4b) are alternative regression models with respect to the corresponding relations (3a) and (4a), but with a more direct dependence on K_{dp}. The functions $f_p(D_z)$, where the subscript p indicates the corresponding parameter, are third-degree rational polynomial functions that were found to adequately describe the Mie character of scattering and to include most of the dependence on D_z

$$f_p(D_z) = \frac{\sum_{n=0}^{3} a_n D_z^n}{\sum_{n=0}^{3} b_n D_z^n}. \quad (5)$$

The coefficients of the polynomials in the numerator and denominator of $f_p(D_z)$ are given in Table I for each relation. In [15] a constraining function of the shape parameter μ of the DSD against the median volume diameter D_0 of raindrops was used for the estimation of other rain parameters, such as DSD parameters and rainfall rate. However, it was shown that the above parameterizations of δ_b, A_h, and A_{dp} from radar observables are independent of the shape parameter μ and this constraint. This independence is due to the use of D_z in the parameterizations.

B. Iterative Solution Scheme

Fig. 1 shows the iterative scheme that is used to implement the SCOP attenuation correction algorithm along a radar ray, where r indicates the range along the ray. The initial guess of the path attenuation corrections dZ_h and dZ_{dr} of Z_h and Z_{dr}, respectively, is the simple linear dependence on Φ_{dp}, with values 0.246 and 0.039 (dB deg^{-1}) for the proportionality coefficients a_h and a_{dp}, respectively, which were found as average values from the simulations in [15] and similar to

TABLE I
VALUES OF THE COEFFICIENTS OF THE RATIONAL POLYNOMIAL FUNCTIONS (5) IN THE PARAMETERIZATIONS OF RAIN PARAMETERS BY (1A)–(4) AT X-BAND (9.37 GHZ) WITH 10 °C AIR TEMPERATURE

Function	a_0/b_0	a_1/b_1	a_2/b_2	a_3/b_3
fD_{z1} in (1a)	0.9190/1.0000	0.1501/−0.2248	−0.1722/0.0182	0.0511/0.0238
fD_{z2} in (1b)	0.0546/0.0012	0.1056/ 0.0361	−0.1587/-0.0180	0.0976/−0.0084
$f\delta_b$ in (2)	−1.0000/1.0000	3.9903/−0.6011	−3.5131/0.0381	0.9494/0.0425
fA_{h1} in (3a)	−1.0000/1.0000	4.2921/−1.0894	−3.8226/0.3431	1.0380/−0.0123
fA_{h2} in (3b)	1.0000/1.0000	4.4689/−0.5402	−4.2310/0.1012	1.5102/ 0.0091
fA_{dp1} in (4a)	−1.0000/1.0000	5.2774/−0.5257	−2.3457/0.0948	0.3165/−0.0036
fA_{dp2} in (4b)	1.0000/1.0000	1.1659/−0.9058	−1.8684/0.2727	0.6931/−0.0044

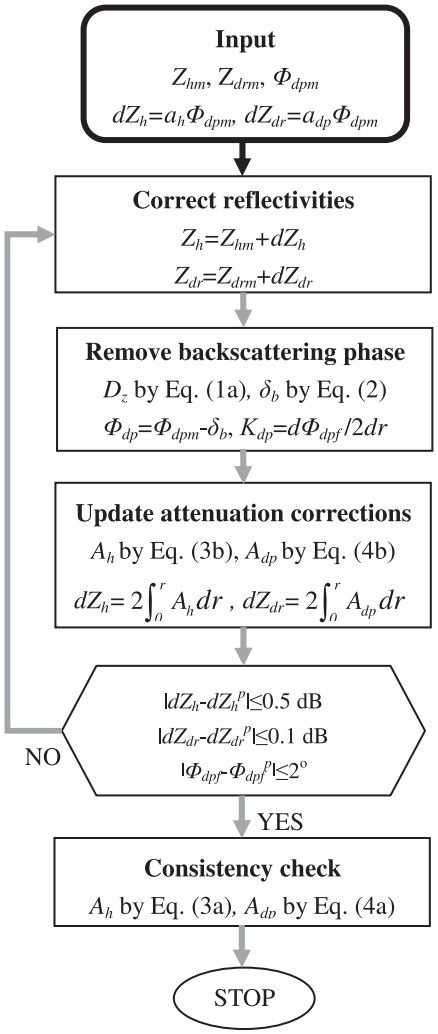

Fig. 1. Block diagram of the attenuation correction iterative algorithm. The superscript p indicates the solution estimated in the previous iteration.

the corresponding equilibrium values found by [2], [4], [7], and [13]. The initial values of dZ_h and dZ_{dr} are not critical for the algorithm. Tests with variable initial guesses showed that the algorithm is stable. The iterations are not made by simply propagating the attenuation correction from the previous range gate to the next, but in each iteration the specific attenuations (and the backscattering differential phase shift) are estimated from the current values of radar observables at all range gates of the radar ray and then the radar observables are updated. A similar iterative scheme, but with different parameterizations, was used by [16] for attenuation correction of radar reflectivities at C-band.

The inputs into the SCOP algorithm are the radar-measured (attenuated) horizontal-polarization reflectivity (Z_{hm}), the differential reflectivity (Z_{drm}), and the differential phase shift (Φ_{dpm}), which includes the backscattering differential phase shift δ_b. A quality control preprocessing step is performed on the measured Φ_{dpm} in order to interpolate the nonsignal parts of the ray with a steady phase value according to adjacent signal data. The measured specific differential propagation phase shift K_{dpm} is estimated from half the radial gradient of Φ_{dpm} after a low-pass Savitzky–Golay linear polynomial filtering of 2 km in length (a 3-km-long filter gave similar results) in order to reduce the noise of the estimated K_{dpm}. The noise of the Φ_{dpm} data used in this paper has a typical standard deviation of 1.5°, which for a 2-km linear filter corresponds (according to [1]) to a random noise in K_{dpm} with a standard deviation of 0.35° km^{-1}. The algorithm estimates δ_b according to (2) and removes it from Φ_{dpm} in order to estimate the "true" Φ_{dp}. The "true" K_{dp} (deg km^{-1}) is then calculated from Φ_{dp} (after filtering it as above) to estimate Φ_{dpf}

$$K_{dp} = d\Phi_{dpf}/2dr = dF_{\mathrm{SG}}(\Phi_{dp})/2dr = dF_{\mathrm{SG}}(\Phi_{dpm}-\delta_b)/2dr \quad (6)$$

where F_{SG} is the Savitzky–Golay range filter function. The two-way path attenuation corrections dZ_h (dB) and dZ_{dr} (dB) are updated by integrating along range r the specific attenuations A_h and A_{dp}, derived from (3b) and (4b), respectively

$$dZ_h = Z_h - Z_{hm} = 2\int_0^r A_h dr; \quad dZ_{dr} = Z_{dr} - Z_{drm} = 2\int_0^r A_{dp}dr \quad (7)$$

where all quantities are expressed in logarithmic units. Equations (3b) and (4b) have a linear direct dependence on K_{dp} with a variable proportionality coefficient along the range, which means that the attenuation corrections (derived as range integration of A_h and A_{dp}) are approximately proportional to the less noisy Φ_{dp} (derived as range integration of K_{dp}) and, thus, the total attenuations will have a better convergence than using (3a) and (4a), which have a direct proportionality to the attenuation affected Z_h, to estimate the specific attenuations.

Furthermore, in order to avoid possible problems in the convergence of the iterative scheme due to radar calibration or measurement errors, the upper limits for A_h, A_{dp}, and δ_b were set to 1.1 K_{dp}, 0.15 K_{dp}, and 25°, respectively, according to the T-matrix simulations in [15]. In this way, the total Φ_{dpm} actually acts as a constraint on the total attenuation correction. The co-polar correlation coefficient ρ_{hv} is not directly used in the attenuation correction algorithm. However, a ρ_{hv} threshold of 0.6 is used to identify nonrain regions and to set the attenuation correction to zero in these regions in order to avoid noise effects on the attenuation correction algorithm.

The iterative scheme converges for the entire radar ray after about five iterations with the following criteria for the convergence of dZ_h, dZ_{dr}, and the filtered Φ_{dpf}:

$$|dZ_h - dZ_h{}^p| \le 0.5 \text{ dB}; \qquad |dZ_{dr} - dZ_{dr}{}^p| \le 0.1 \text{ dB};$$
$$|\Phi_{dpf} - \Phi_{dpf}{}^p| \le 2^\circ \tag{8}$$

where the superscript p indicates the solution estimated in the previous iteration. The computation time is quite small, as only direct calculations for the entire radar ray are involved without the need to solve time-consuming minimization problems as in previous attenuation correction methods. This is due to the improved parameterizations of A_h, A_{dp}, and δ_b with minimum parameterization error. For this reason, the iterative scheme actually solves a nonlinear system of consistent equations with as many unknowns, which are the A_h, A_{dp}, and δ_b values or equivalently the dZ_h, dZ_{dr}, and Φ_{dp} at each range gate, as inputs (the corresponding measurements of Z_{hm}, Z_{drm}, and Φ_{dpm}). The initial unknown values are expected to be close to the actual solution and, thus, the iterative scheme should converge to it.

According to [15], the bias and random error of the A_h and A_{dp} parameterizations in (3) and (4), due to typical radar calibration bias and measurement noise (1 dB, 0.2 dB, and 0.3 deg km^{-1} for Z_h, Z_{dr}, and K_{dp}, respectively), are less than 20%. This is also about the maximum expected relative error of accumulated A_h and A_{dp}, i.e., of dZ_h and dZ_{dr}. A real-time method to improve the calibration of Z_{dr} is to estimate it in each radar scan at low elevation angles using a Z_{dr} approximation from an average Z_h–Z_{dr} relation Z_{dre} (Z_h) such as the one presented by [7]

$$\begin{aligned} Z_{dr} \text{ bias} &= < Z_{dre}(Z_h) - Z_{drm} > \\ &= 0.0528 < Z_{hm} > -0.511 - < Z_{drm} >, \\ &\qquad \text{for } 15 \le Z_{hm} \le 25 \text{ dBZ and } \Phi_{dpm} \le 3^\circ \end{aligned} \tag{9}$$

where the operator <> indicates the average value in the radar scan. The use of a range of small Z_{hm} aims at the selection of good signal data with small expected true Z_{dr} values (about 0.5 dB on average). The restriction to small Φ_{dpm} shift aims at the selection of data with very small signal attenuation. When this method was applied to our radar data (Section III), a temporal slow (i.e., not random) variation of ±0.5 dB around a mean value in Z_{dr} calibration was found. Its application is shown to improve considerably the performance of the attenuation correction algorithm when compared to the disdrometer data in Section III. A constant calibration bias was applied to the radar reflectivity Z_h. This calibration bias was determined through comparison with X-band reflectivity values calculated from comparison with the disdrometer data at low rain-path attenuation (less than 0.5 dB) and in the range of 15–30 dBZ of the Z_h values from the disdrometer.

After the exit from the iterative scheme, a consistency check of the range profiles is carried out by comparing the estimation of A_h and A_{dp} given by (3a) and (4a) with the corresponding estimates from (3b) and (4b), which are used in the iterative scheme. A simple implementation of such a consistency check is to compare the path attenuations dZ_h and dZ_{dr} estimated from the two sets of equations with an upper limit of 2 dB for the dZ_h difference and 0.4 for the dZ_{dr} difference (i.e., twice the expected error of Z_h and Z_{dr}, respectively) in order to accept the profiles up to the range that these limits are not exceeded. Failure of such a self-consistency of the algorithm implies (if the measurement noise is not too high) that assumptions like the normalized Gamma function for the DSD, the function of drop axis ratio, and the canting angle distribution made in the T-matrix simulations in [15], which were used to find the parameterization functions in (1)–(4), do not hold for some parts of the radar ray. This could be due to the presence of hail or snow in those cells. In this case, a bad quality flag is attached to the retrieved range profiles. A similar approach to detect hail in the radar ray based on the failure of a model of polarimetric observables that should be valid only in rain was proposed by [11]. Also, the observed combination of a high value of the proportionality coefficient between A_{dp} and K_{dp} and a low value of the co-polar correlation coefficient ρ_{hv} outside the range of values expected in rain was proposed by [17] as a method to detect hail (possibly melting) in strong attenuating rain cells.

III. Evaluation Against Disdrometer Data

Two years' worth (2008-2009) of data were collected in Athens (Greece) with the mobile Doppler dual polarization radar (X-Pol) operating at X-band 9.37 GHz and the bidimensional video disdrometer (2D-VD) of the National Observatory of Athens. The radar is a subsequent version of the system described by [18]. The radar beam width is about 1°, and typical operating parameters are: a pulse repetition frequency of 1 kHz, a pulse length of 1 μs (peak power about 30 kW per polarization), and an antenna rotation rate of 6° s^{-1} in plan-position indicator (PPI) scans and 3° s^{-1} in range-height indicator (RHI) scans. The noise values of polarimetric observables are the typical values already given in Section II-B. For the X-Pol radar, ρ_{hv} value in rain reaches 0.995 and is usually above 0.8. Rain signal data is determined as the data with signal power above the noise level of about −110 dBm for X-Pol radar and ρ_{hv} greater than 0.6. Possible ground clutter is detected and rejected in regions where, in addition to value of ρ_{hv} lower than 0.6, the radial Doppler velocity is less than 1 ms^{-1} and the spectrum width is less than 1 ms^{-1}. These are the maximum expected values [19] for ground clutter from stationary rigid targets, vibrating foliage, etc., and a rotating radar antenna with a rotation rate for X-Pol data up to 6° s^{-1} in PPI scans. A 15-dB four-pole IIR filter for

clutter suppression [18] is also applied to the radar in-phase and the quadrature-phase components of the radar signal in real time.

The version of the video disdrometer (2D-VD) is the one described by [20]. The disdrometer is calibrated regularly by dropping metallic calibration balls through the measurement area. The disdrometer DSD data are in time intervals of about 1 min and represent a diameter range of 0.1–10 mm with a bin resolution of 0.2 mm. The resolution of the raindrop size depends on the detection position in the measurement area and the fall velocity of the raindrop, but on average it is about 0.2 mm (thus, the first diameter bin is empty). Raindrops larger than 10 mm were rare in the dataset used in this paper (D_0 values were less than 2.5 for 99.5% of the cases) and the minimum D_0 was 0.5 mm. Using the above diameter bins, the error on the retrieved (using DSD moments) DSD parameters due to the truncation of the DSD is very small (less than 5%) for $0.4 < D_0 < 2.5$ mm [21]). As was noted in [20], flow distortion by the disdrometer due to its height (about 1.2 m) under significant horizontal wind and drop splashing is the main possible under-catchment errors. Sampling errors may also occur especially for large drops due to the relatively small measurement area (10×10 cm). Quality control was applied to the raw detected particles using various criteria. Bad detections were rejected if there was more than 40% difference between the measured fall velocity and the value corresponding to the measured equivolumetric diameter of the particle according to the empirical relations [1] as in [20]. The video disdrometer records the shape (outline) and the fall velocity of the particles passing though the measurement area. The shape of the particles is corrected for the effects of horizontal motion and orientation (canting angle) using the assumption of a rotational symmetry axis for each particle [22], [23]. Using the shape information, particles with irregular shape like the ones with a few points (fewer than six points) in their outline or a very high estimated canting angle (larger than 45°) were also rejected. After this quality control, a normalized Gamma distribution could be fitted to the estimated DSD starting from diameter values of 0.5 mm.

The radar was installed at the northern suburbs of Athens at an altitude of 500 m above mean sea level, and the 2D-VD with two rain gauges was deployed to the south at distance 35 km away from the radar at an altitude of 12 m. There are no terrain obstacles in the path from the radar to the disdrometer. The volume scan of the radar included PPI scans at low elevation angles (0°, 0.5°, and 1°) and RHI scans above the 2D-VD (about 2 min for a full volume scan depending on scanning geometry in each event). The 2D-VD can also provide after processing of raw data estimates of shape (axis ratio) and orientation (canting) of raindrops in addition to DSD spectra but these estimates are noisy and excluded from the data analysis. Instead, a Fisher distribution with a standard deviation of 7.5° (the middle of the possible range of 5°–10° according to [1]) for canting angle distribution and a raindrop axis ratio according to [24] were assumed. These assumptions and the measured DSD spectra from the disdrometer were used in T-matrix scattering calculations [25] for an air temperature of 10 °C to estimate radar observables (reflectivities) at the disdrometer position.

In the comparison between radar and disdrometer, the radar measurement volume above the disdrometer was used. The time delay due to the raindrops falling from the altitude of the radar sampling volume above the disdrometer to the altitude of the disdrometer is taken into account using the terminal velocity estimated from relations described in [1] at the median volume diameter, which was estimated by the microphysical algorithms [15]. The effect of horizontal wind (horizontal advection of the raindrops) was not considered directly, but instead it was assumed that it is included in the synchronization between the time series of each rain event (the time duration of rain events was usually some hours) of reflectivity measurements of Z_h in the radar sampling volume and Z_h estimated from the disdrometer. The time delay was found as the time lag with the maximum correlation between these two time series. Liner interpolation of the disdrometer time series was used in the above synchronization with the radar measurements. In addition, a spatial averaging was applied to the radar measurements using the adjacent (± 1) radar gates and rays. The radar gate length was 150 m and, at the range of the 2D-VD (about 35 km), the azimuth resolution of radar rays (0.6°) corresponds to 365 m. A moving average of adjacent measurements was applied to the disdrometer time series in order to reduce the noise due to sampling errors. This spatial averaging (450 m along the ray and 1100 m perpendicularly to the ray) of the radar measurements and the temporal averaging (about 3 min) of the 2D-VD measurements reduced also the possible error from the horizontal advection of the drops due to the wind. The observed rain intensities ranged from light stratiform rain events to short-duration heavy convective storms. The radar sampling volume, which is used in the comparison with the disdrometer during stratiform rain events, is in most cases below the melting layer (bright band) and, thus, it is expected that the rain field does not change significantly along the vertical distance between the disdrometer and the radar sampling volume.

A. Range Profiles and Time Series

Fig. 2 shows sample range profiles of Z_h, Z_{dr}, and Φ_{dp} during a winter storm event and the corrected radar parameters after the application of the described algorithm as well as other algorithms found in the literature. The range resolution is 150 m. Raw data correspond to the measured (uncorrected) radar parameters, SCOP corresponds to data after correction with the algorithm of Fig. 1, ZPHI (Z_h–Φ_{dp}) represents data after correction with the algorithm of [4], and FSC (full self-consistent) represents data after correction with the algorithm of [13] and [14] for X-band. The horizontal-polarization reflectivity Z_h corrections by SCOP and ZPHI agree with the disdrometer calculation, which is located at a distance of about 5 km behind a reflectivity peak of about 60 dBZ. The FSC algorithm gave a correction at the 2D-VD range about 5 dB lower than the other algorithms, which is a general observation (Fig. 4 in Section III-B) and it is probably due to the parameterization functions used in this algorithm.

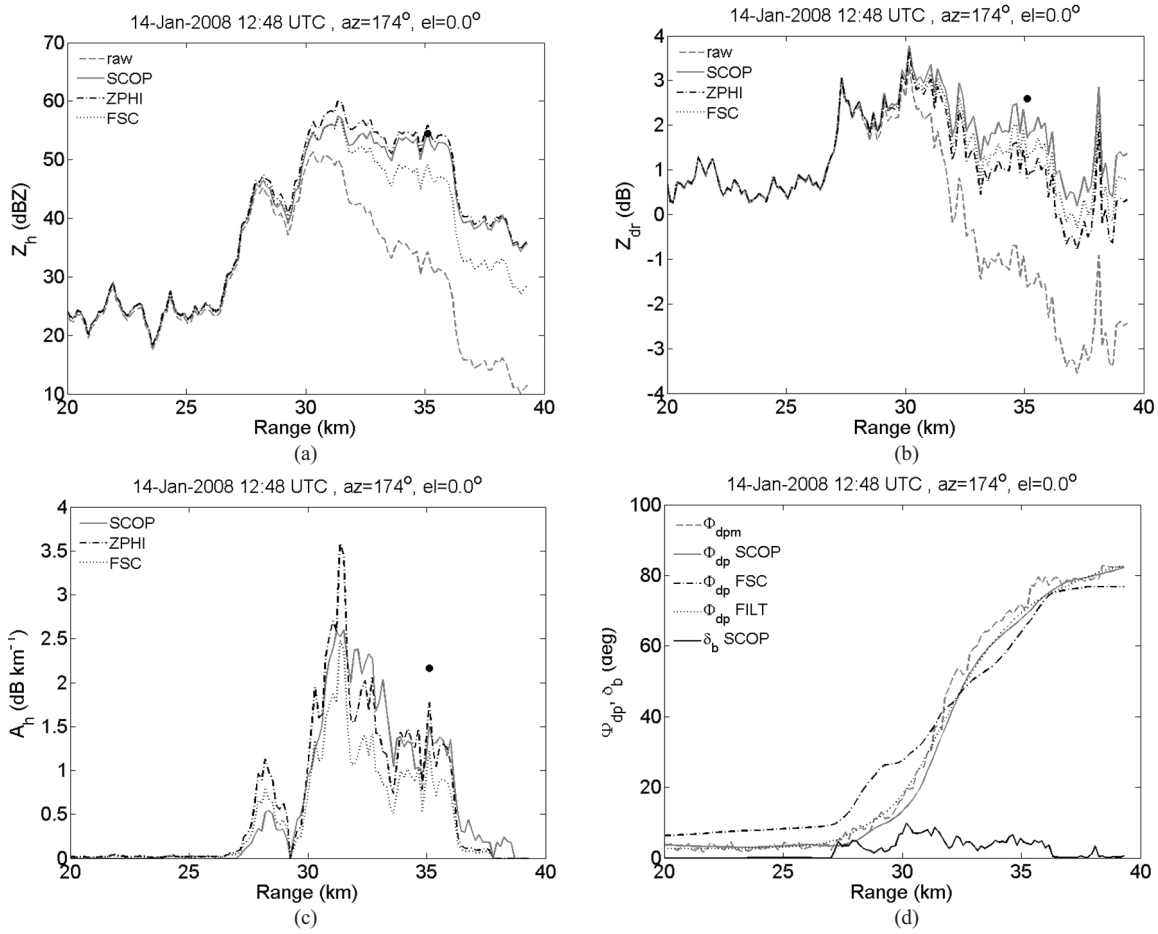

Fig. 2. Range profiles of (a) Z_h, (b) Z_{dr}, (c) A_h, and (d) Φ_{dp} and δ_b before (raw) and after application of attenuation correction algorithms SCOP, ZPHI, and FSC. The solid circles correspond to the values calculated from the disdrometer measurements.

The Z_h profile from the FSC algorithm also shows a negative trend behind the reflectivity peak but the other two algorithms show nearly steady reflectivity, which is probably expected to occur in the actual profile. The differential reflectivity Z_{dr} corrections exhibit underestimation (less for the SCOP algorithm) with respect to the disdrometer-derived Z_{dr} values, which is also a general trend in the data. Despite the underestimation exhibited for Z_{dr}, the improvement of radar Z_{dr} values after the attenuation correction from all methods is significant especially in the range of the most negative measured value of about -3.5 dB, which is due to the strong attenuation at the storm peak. Even though the Z_h profiles by SCOP and ZPHI algorithms look similar, the estimated specific attenuation A_h profiles in Fig. 2(c) do not. Thus, the details of the Z_h profiles are not the same and the peak values differ by about 3 dB. It should be noted that, as expected, the ZPHI profile does not fulfill the self-consistency of the minimum error parameterizations in (1)–(4).

The lower values of estimated A_h by the correction methods when compared to the disdrometer-derived values are probably due to the smoothing (a 2-km length was used for the low-pass filter mentioned in Section II-B) of the Φ_{dp} profile shown in Fig. 2(d) and, thus, to the reduction of K_{dp} peaks. In this figure, FILT represents the Φ_{dp} from a filtering method similar to the one presented by [26], which aims to remove as much as possible the δ_b effect from the measured differential phase shift Φ_{dpm}. It can be seen that the results of this method agree with Φ_{dp} estimated by the SCOP algorithm at ranges well behind the reflectivity peak where the Φ_{dp} slope is reducing. However, the results of this method at the beginning of the rain cell and the reflectivity peak are different from those by the SCOP algorithm and follow the measured Φ_{dpm}, whereas the backscattering phase δ_b as estimated by the SCOP algorithm is significant (up to 10°). The Φ_{dp} estimated by the FSC algorithm is clearly in error, which is due to the parameterization functions and the constraining method adopted in this algorithm, i.e., least-square error minimization of the difference between the estimated Φ_{dp} and measured Φ_{dp} by introducing a multiplicative factor on the ZPHI estimation of specific attenuation.

Fig. 3 shows the uncorrected (raw) and corrected with the SCOP algorithm reflectivities Z_h and Z_{dr} from the 0° elevation PPI scan that corresponds to the range profiles of Fig. 2. A narrow 1000-m-high mountain at about a 210° azimuth angle and 10-km range was the main obstacle in the 180°-wide sector where the radar (located at an altitude of 500 m) was scanning, while the north and northwest directions were completely blocked by other mountains. The storm front approached the area from the south, and only the part of the PPI scan that includes this front is shown for higher

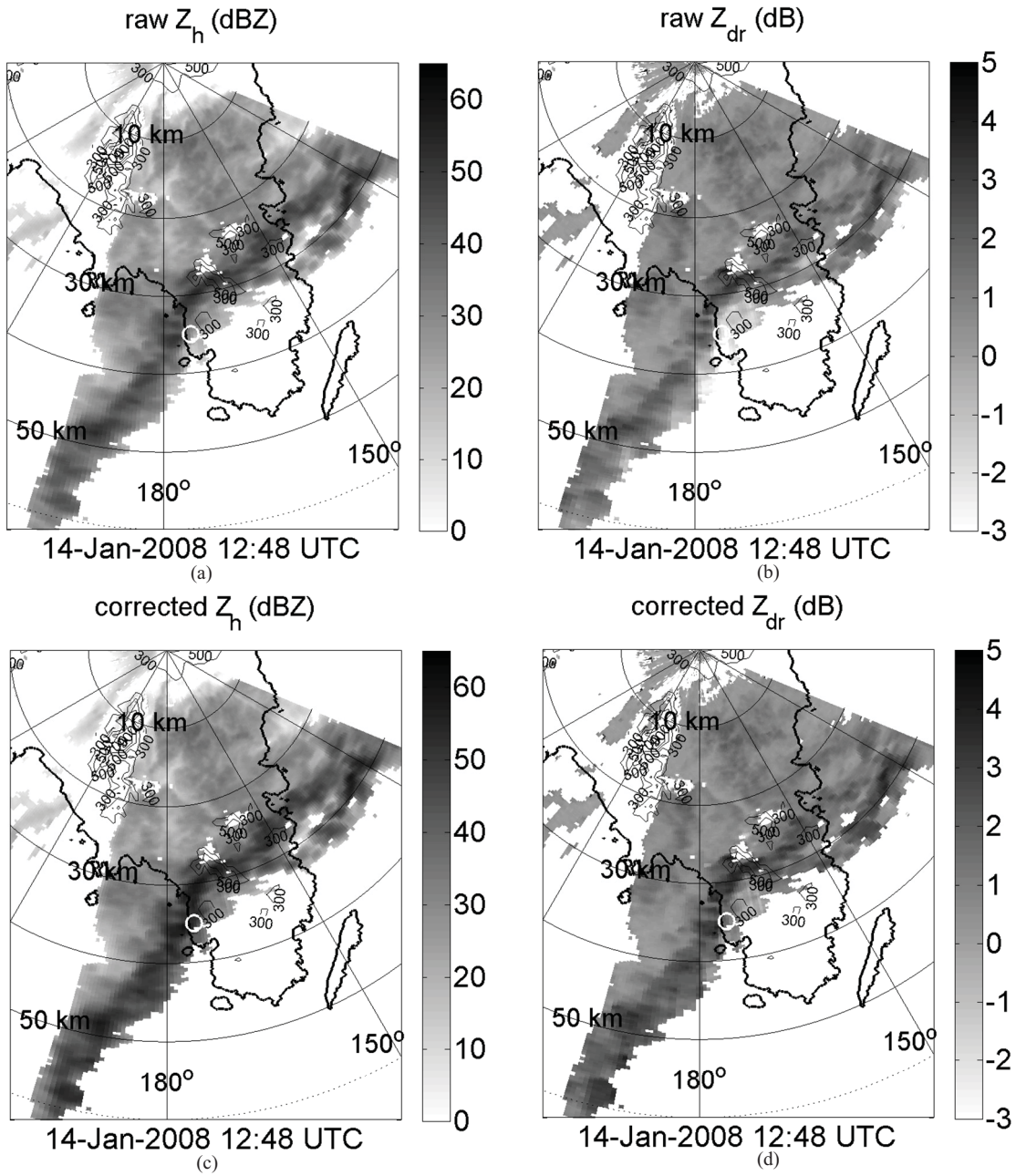

Fig. 3. Raw uncorrected (a) Z_h and (b) Z_{dr} from the PPI scan that corresponds to the range profiles shown in Fig. 2 at an antenna elevation angle of 0°. Plots (c) and (d) are the corresponding Z_h and Z_{dr} corrected for rain-path attenuation with the SCOP algorithm. The white circle indicates the position of the disdrometer. In the first figure, terrain elevation above sea level is shown with contours and labels in meters and the coastline is shown with thick lines.

resolution purposes. No algorithm parameters are tuned in each radar ray or rain cell in the SCOP algorithm and, thus, the attenuation correction is smooth (no discontinuities) in range and azimuth. Thus, additional smoothing techniques are not required in contrast to attenuation correction algorithms that use minimization-variational approaches for parameter tuning in each radar ray as described by [11]. The attenuation correction of Z_h and Z_{dr} in the front zone is quite high, as shown in Fig. 2, and measured negative values of Z_{dr} behind the front in the azimuth directions 165° to 175° and ranges 30 to 35 km (i.e., at the disdrometer site and to the east of it) are corrected to generally positive values. The exception to this is at about 165° azimuth and 32-km range where nonsignal data (indicated with missing data) just ahead of the front zone were detected using the criteria (based mainly on ρ_{hv} values) described in the beginning of Section III. This nonsignal area, as well as other small areas of missing data that match with the terrain, is due to ground clutter that remains after filtering. These are the only radar rays in the PPI scan where the consistency check described at the end of Section II-B failed. As mentioned in the description of the iterative scheme in Section II-B, the SCOP algorithm has a good convergence because of the linear direct dependence of (3b) and (4b) (which are used to parameterize the specific attenuations) on K_{dp}. Thus, problems like remaining ground clutter, partial beam blockage, or occurrence of other water phases (like hail or

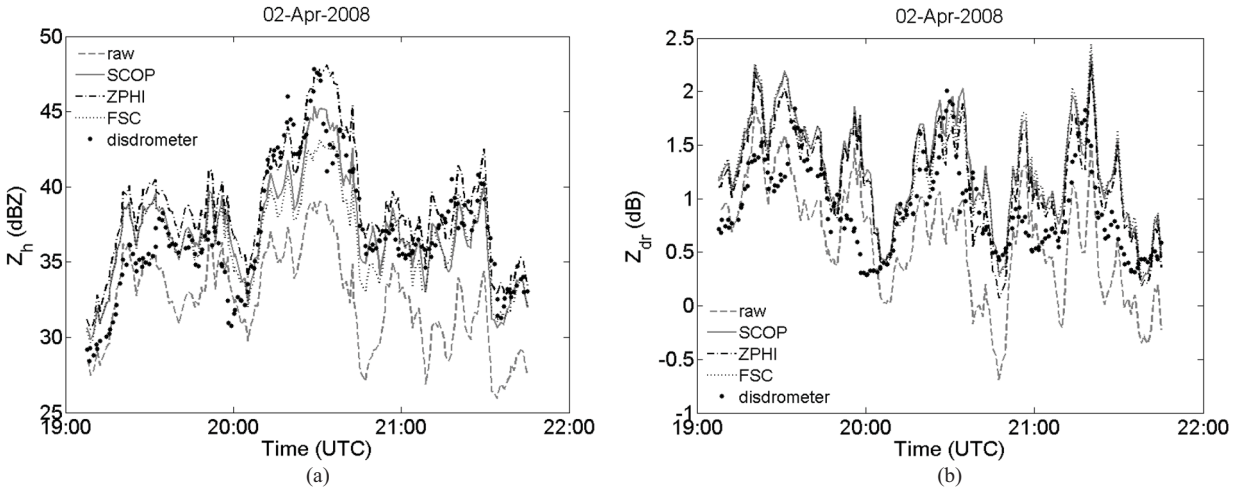

Fig. 4. Time series of (a) Z_h and (b) Z_{dr} before (raw) and after application of attenuation correction algorithms SCOP, ZPHI, and FSC during a rain event. Dots correspond to the values calculated from the disdrometer measurements.

snow) in the propagation path do not cause the algorithm to diverge, but result in incorrect estimation of the attenuation correction. Behind the front, the strong attenuation at X-band reduces the radar signal to noise level and, thus, possible rain structure far behind the front is not observable.

Fig. 4 shows time series of the reflectivities Z_h and Z_{dr} from the various attenuation correction algorithms and the disdrometer during a rain event with moderate values of reflectivity. All correction algorithms improve considerably the radar measurements. The highest peak in the time series of the disdrometer Z_h agrees with ZPHI, but ZPHI continues to show high Z_h values after the peak. Generally for Z_h the ZPHI algorithm exhibits higher values than the SCOP algorithm, whereas the FSC algorithm gives values systematically lower than both SCOP and ZPHI. All algorithms give similar Z_{dr} values. The radar values of Z_h and Z_{dr} follow well the corresponding disdrometer-derived values for most of the time. However, there are time periods when the variations in disdrometer values are not correlated with the variations in the radar data, and in some time periods (like in the beginning of the event) they are similar to or smaller than the uncorrected (raw) radar values. This implies that the difference in altitude between the disdrometer and the radar sampling volume above the disdrometer may lead (e.g., during high winds or proximity of the radar sampling volume to the melting layer) to significant errors in the comparison, which will produce considerable scatter. Also, the attenuation by the wetting of the radar antenna dish during rainfall in the area of the radar can affect significantly the self-consistent algorithms like SCOP and FSC. This was observed in some rain events and appeared as significant change (drop of measured Z_h by up to 6 dB depending on rainfall rate) in the calibration bias of Z_h with respect to the disdrometer. It should be noted that the ZPHI algorithm is immune to radar calibration error for the attenuation correction of Z_h [4], but it is sensitive to radar calibration error for the attenuation correction of Z_{dr}.

B. Statistical Results

In order to reduce errors in the evaluation of the performance metrics of the attenuation correction algorithms due to sampling differences and the separation in altitude between the disdrometer and the radar sampling volume or other reasons like antenna wetting, a proper selection of rain events was applied. Only rain events with correlation between the disdrometer and the radar horizontal reflectivities higher than 0.7 and measured (raw) radar reflectivity Z_{hm} less than or up to 3 dB higher than the disdrometer value Z_{hD} for at least 50% of the event points were used. The second selection criterion was applied in order to remove data with Z_{hm} higher than Z_{hD}, which occurred when the melting layer (bright band) was very low (at about 1000 m above mean sea level) in some rain events. The SCOP algorithm (as with the rest of the attenuation correction algorithm mentioned in the introduction) is based on (1)–(4), which do not apply to the melting layer but only to rain regions. In the remaining cases, it is expected that Z_{hm} is less than Z_{hD} due to path attenuation with a tolerance of 3 dB to account for the measurement noise with a standard deviation of about 1.5 dB in Z_{hD}. In addition, in order to remove noisy disdrometer data due to low rainfall rate, a lower limit of 15 dBZ was set for the horizontal-polarization reflectivity calculated by the 2D-VD data.

A total of 1498 rain data points from 18 rain events were finally selected according to the criteria mentioned above. The values of the 2D-VD-derived horizontal-polarization reflectivity (Z_{hD}) and differential reflectivity (Z_{drD}) values in this dataset were up to 61 dBZ and 3.7 dB, respectively. Overall, the dataset was mostly comprised of stratiform rain events, and only three events could be characterized as convective (with reflectivity values above 50 dBZ in isolated rain cells). This can be concluded by Fig. 5, where most of the Z_h and Z_{dr} attenuation values are less than 10 and 1 dB, respectively. We did not remove data in order to make a balance between the two rain event types, which would decrease significantly the total number of data points. Instead, we show all data and discuss the differences in attenuation correction performance at low attenuation values (stratiform rain events) and high attenuation values (convective rain events). Fig. 5 shows the scatter plots of the attenuation correction by the various algorithms against the reference attenuation value estimated as the difference between the

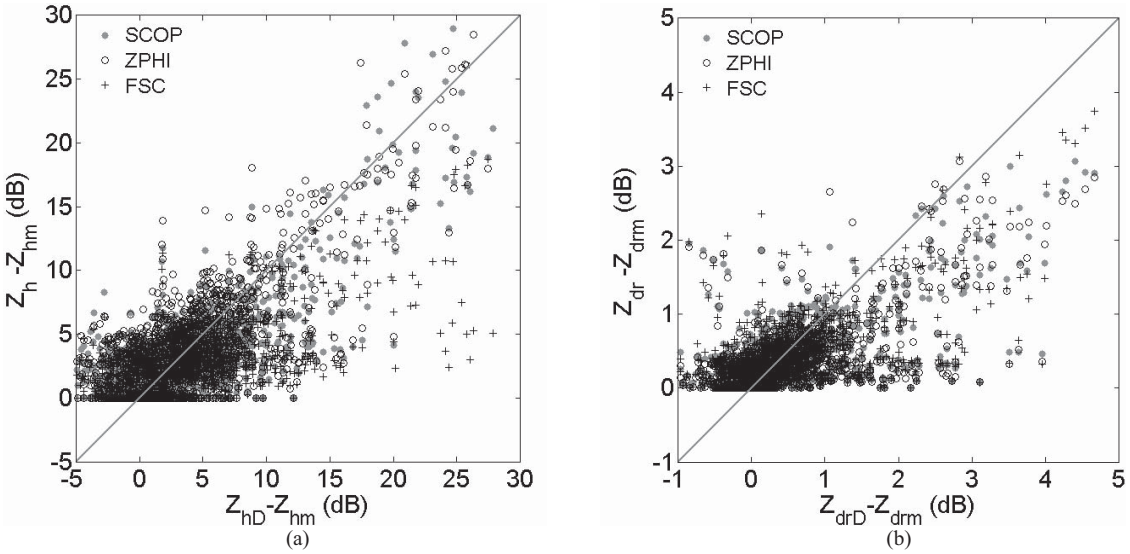

Fig. 5. Scatter plots of the radar attenuation corrections (a) Z_h–Z_{hm} and (b) Z_{dr}–Z_{drm} estimated from the SCOP, ZPHI, and FSC algorithms against the corresponding reference attenuations Z_{hD}–Z_h and Z_{drD}–Z_{drm} calculated from the disdrometer measurements.

2D-VD-derived radar observables and the radar-measured values Z_{hm} and Z_{drm}.

There are data points with Z_{hD} less than Z_{hm} and Z_{drD} less than Z_{drm}, which are due to noise in the measurements (especially in the disdrometer data). In general, the results are consistent with Figs. 2 and 4. For Z_h corrections, the ZPHI algorithm seems to give on average corrections closer to the reference values above 10 dB and the SCOP algorithm gives slightly lower corrections for this range of corrections, whereas the FSC algorithm gives generally lower corrections. For the data shown in Fig. 5, the failure of the consistency check of the SCOP algorithm described at the end of Section II-B was about 3%, which mainly includes convective storm cells with possible hail (reflectivity values higher than 50 dBZ) at various ranges along the path of the radar beam up to the disdrometer. In order not to bias the statistics presented below in terms of the large number of small attenuation corrections as seen in Fig. 5, lower limits of 2 and 0.4 dB (twice the noise level in radar measurements) were set for the attenuation corrections of Z_h and Z_{dr} by the SCOP algorithm, respectively. In addition, the data with Z_{hD} and Z_{drD} less than Z_{hm} and Z_{drm}, respectively, were removed because this is not the expected actual behavior as mentioned above. A total of 478 rain data points satisfied these criteria.

The correlation coefficient for all algorithms is about 0.8, the normalized standard (root-mean-square) error (NSE), where the normalization is done with respect to the reference (2D-VD) mean value of the corresponding parameter, is about 50%, with worse numbers for the FSC algorithm. The normalized mean bias (NB) is -12% for the SCOP algorithm, 6% for the ZPHI algorithm, and -32% for the FSC algorithm. The small underestimation by the SCOP algorithm is probably due to the smoothing of the Φ_{dp} profile for noise reduction before the estimation of its half gradient K_{dp} as mentioned in Section II-B. For Z_{dr} corrections, all algorithms show a clear underestimation for path attenuation values above 1 dB. The statistical numbers for Z_{dr} corrections are similar correlation coefficient and NSE error for all algorithms as with the Z_h corrections and NB errors of -17%, -27%, and -17% for SCOP, ZPHI, and FSC algorithms, respectively. This underestimation occurred mainly when the measured radar differential reflectivity Z_{drm} was below $-1\ dB$. When only the attenuation corrections for this range of Z_{drm} values are considered, the underestimation (NB errors) of the Z_{dr} corrections is about -40% for all algorithms, whereas the Z_h corrections do not show different NB errors than the overall statistics derived from the entire dataset. The cases with such highly negative Z_{drm} were observed during strong attenuation behind 50 dBZ or higher reflectivity peaks. Thus, a plausible explanation for this underestimation could be that melting hail was present at some parts along the path of the radar beam (even though the consistency test described at the end of Section II-B did not fail in most of those cases), which is not considered in the algorithms described herein. The performance of FSC algorithm against ZPHI algorithm was examined in [13] and [14] using the X-band profiles generated (based on scattering simulations) from S-band radar data. It was found that the ZPHI algorithm estimated larger attenuation corrections with respect to the FSC algorithm, which is a similar trend with the one observed here in the comparison with *in situ* disdrometer data but with the opposite conclusion.

As was noted in Section III-A, despite the underestimation of Z_{dr}, the improvement of raw uncorrected values is significant. Fig. 6 shows the occurrence frequency plots of the difference between uncorrected (raw), SCOP, ZPHI, and FSC corrected radar observables (Z_h and Z_{dr}) and the corresponding reference values derived from the 2D-VD (Z_{hD} and Z_{drD}). In order not to bias the histograms, the same lower limits for the attenuation corrections were used as in the estimation of NB and NSE metrics mentioned above. The improvement of the histograms before and after the

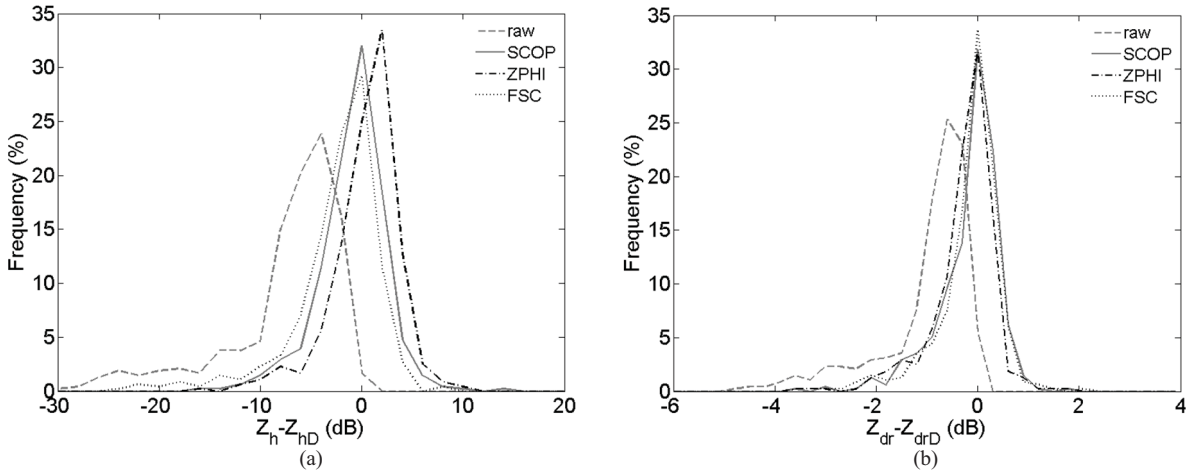

Fig. 6. Occurrence frequency of the difference between raw, SCOP, ZPHI, and FSC corrected radar observables (a) Z_h and (b) Z_{dr} and the corresponding values Z_{hD} and Z_{drD} calculated from the disdrometer measurements.

attenuation corrections is evident. On average, the difference of radar Z_h values from the corresponding disdrometer-derived values is -7.4 dB before attenuation correction and becomes -0.9, 0.4, and -2.4 dB after the application of SCOP, ZPHI, and FSC attenuation corrections, respectively, which is in agreement with the discussion for the scatter plot in Fig. 5(a). However, the mode of the distributions, which corresponds to the most frequent attenuation value of about 5 dB, occurs at a difference value of 2 dB for ZPHI algorithm, instead of zero as for the other two algorithms. Thus, at low attenuations, ZPHI algorithm systematically overestimates the attenuation correction of Z_h. The corresponding numbers for Z_{dr} differences are -1.0 dB before the attenuation correction and -0.2, -0.3, and -0.2 dB after the application of SCOP, ZPHI, and FSC attenuation corrections, respectively. The left tail of the histograms, which is given as the 10% quantile value (cumulative probability) below, is more extended than the right one especially for the Z_h correction with the FSC algorithm, which is due to the underestimation of attenuation corrections as presented in Fig. 5. The spread of the histograms for Z_h differences using the 10% and 90% quantiles (shown in parenthesis) is 13.6 $(-15.9, -2.3)$ dB before the attenuation correction and 7.3 $(-4.8, 2.5)$, 7.2 $(-3.3, 3.9)$, and 8.9 $(-7.3, 1.6)$ dB after the application of SCOP, ZPHI, and FSC, respectively. The corresponding numbers for Z_{dr} differences are 2.2 $(-2.4, 0.2)$, 1.4 $(-1.0, 0.4)$, 1.3 $(-1.0, 0.3)$, and 1.4 $(-1.0, 0.4)$ dB, respectively. This spread, which is significant even though it is reduced to about its value after attenuation correction, is attributed to sampling differences (point versus volume measurements) and the reduced correlation between the rain field at the position of the disdrometer and the radar sampling volume (spatial separation). Specifically, at 1° elevation angle (the maximum angle used for this paper), the altitude difference between the 2D-VD and the radar sampling volume is about 1100 m and the radar beam width is about 600 m.

IV. Conclusion

A new self-consistent algorithm for attenuation correction in rain was developed for dual-polarization radars at X-band frequency. The proposed SCOP algorithm applies to low antenna elevation angles and uses optimal parameterizations of specific horizontal and differential attenuation and backscattering phase shift in an iterative scheme. The same attenuation correction algorithm can be applied to other attenuating frequencies (e.g., to C-band) by providing a new estimation of the constants in the parameterizations using T-matrix scattering simulations. The inputs into the iterative scheme are the measured horizontal-polarization reflectivity, differential reflectivity, and differential phase shift. The iterative scheme is applied to the entire radar rays instead of to separate rain cells like in ZPHI and other algorithms found in the literature, without solving any minimization problem and, thus, it is quite fast and stable. For the current radar dataset and the same computing system, the SCOP algorithm is about five times slower than ZPHI and FSC is about seven times slower than ZPHI, while other more complex algorithms like the modified ZPHI algorithm of [6], which requires solving a minimization problem in each radar ray and rain cell, are more than five times slower than the SCOP algorithm.

The performance of the new algorithm was compared with ZPHI and FSC algorithms using disdrometer data. For the attenuation correction of horizontal-polarization reflectivity, the new algorithm shows clearly an improved performance compared to FSC (NB error of -12% compared to -32% of FSC) and similar performance with ZPHI (NB error of 6%). However, ZPHI exhibited an overestimation by about 2 dB at the more frequent low rain-path attenuation values (less than 5 dB). The small underestimation by SCOP is probably due to the 2-km-long filtering of the differential phase shift that is used to reduce its noise and the subsequent reduction of the peaks of the specific differential propagation phase shift. All algorithms showed similar behavior for the attenuation correction of differential reflectivity with a significant (40%) systematic underestimation at rain-path attenuation values higher than 1 dB, which is probably due to the presence of hail in the path of the radar beam during those cases. The inclusion in the algorithm of a detection scheme and parameterization functions of specific attenuations for other water phases, such as hail or melting snow in the melting layer along the

radar ray, could be a future work to alleviate some of these issues.

The ZPHI algorithm (and the FSC algorithm which is based on ZPHI) uses the approximation of a fixed intercept parameter of the DSD in rain cells, and its parameterization functions were estimated for a shape parameter equal to 2 for the DSD and an air temperature of 10 °C. The logarithmic scaling, which was used in ZPHI for the derivation of parameterization functions after normalization by the intercept parameter of the DSD, does not give accurate estimation of radar parameters for variable shape parameter of the DSD or air temperature. On the other hand, the parameterizations of specific attenuations used in the new algorithm are quite accurate (approximation error less than 5%) for a very wide range of values of rain DSD and drop shape parameters and air temperature. This feature makes the SCOP algorithm capable of providing the details of the reflectivity profiles better than the other algorithms. This has to be tested in future studies using more disdrometer data representing different radar ranges and more convective rain events, which were limited in the current dataset. The algorithm requires a relatively good radar calibration, within the range of typical radar calibration bias and measurement noise, to ensure low errors of its results. The differential reflectivity can be calibrated in real time without additional measurements using low-elevation and low-attenuation data and the Z_{dr} approximation from an average Z_h–Z_{dr} relation.

REFERENCES

[1] V. N. Bringi and V. Chandrasekar, *Polarimetric Doppler Weather Radar: Principles and Applications*. Cambridge, MA, USA: Cambridge Univ. Press, 2001, p. 636.

[2] S. Matrosov, K. Clark, B. Martner, and A. Tokay, "X-band polarimetric radar measurements of rainfall," *J. Appl. Meteor.*, vol. 41, pp. 941–952, Sep. 2002.

[3] L. D. Carey, S. A. Rutledge, D. A. Ahijevych, and T. D. Keenan, "Correcting propagation effects in C-band polarimetric radar observations of tropical convection using differential propagation phase," *J. Appl. Meteor.*, vol. 39, no. 9, pp. 1405–1433, 2000.

[4] J. Testud, E. Le Bouar, E. Obligis, and M. Ali-Mehenni, "The rain profiling algorithm applied to polarimetric weather radar," *J. Atmos. Ocean. Technol.*, vol. 17, no. 3, pp. 332–356, 2000.

[5] T. J. Smyth and A. J. Illingworth, "Correction for attenuation of radar reflectivity using polarization data," *Quart. J. Royal Meteorol. Soc.*, vol. 124, no. 551, pp. 2393–2415, Oct. 1998.

[6] V. N. Bringi, T. Keenan, and V. Chandrasekar, "Correcting C-band radar reflectivity and differential reflectivity data for rain attenuation: A self consistent method with constraints," *IEEE Trans. Geosci. Remote Sens.*, vol. 39, no. 9, pp. 1906–1915, Sep. 2001.

[7] S. Park, V. N. Bringi, V. Chandrasekar, M. Maki, and K. Iwanami, "Correction of radar reflectivity and differential reflectivity for rain attenuation at X-band, part I: Theoretical and empirical basis," *J. Atmos. Ocean. Technol.*, vol. 22, no. 11, pp. 1621–1632, Nov. 2005.

[8] S. Park, M. Maki, K. Iwanami, V. N. Bringi, and V. Chandrasekar, "Correction of radar reflectivity and differential reflectivity for rain attenuation at X-band, part II: Evaluation and application," *J. Atmos. Ocean. Technol.*, vol. 22, no. 11, pp. 1633–1655, 2005.

[9] M. N. Anagnostou, E. N. Anagnostou, and J. Vivekanandan, "Correction for rain path specific and differential attenuation of X-band dual-polarization observations," *IEEE Trans. Geosci. Remote Sens.*, vol. 44, no. 9, pp. 2470–2480, Sep. 2006.

[10] F. S. Marzano, G. Botta, and M. Montopoli, "Iterative Bayesian retrieval of hydrometeor content from X-band polarimetric weather radar," *IEEE Trans. Geosci. Remote Sens.*, vol. 48, no. 8, pp. 3059–3074, Aug. 2010.

[11] R. J. Hogan, "A variational scheme for retrieving rainfall rate and hail reflectivity fraction from polarization radar," *J. Appl. Meteorol. Climatol.*, vol. 46, no. 10, pp. 1544–1564, Oct. 2007.

[12] M. Schneebeli and A. Berne, "An extended Kalman filter framework for polarimetric X-band weather radar data processing," *J. Atmos. Ocean. Technol.*, vol. 29, no. 5, pp. 711–730, May 2012.

[13] E. Gorgucci, V. Chandrasekar, and L. Baldini, "Correction of X-band radar observation for propagation effects based on the self-consistency principle," *J. Atmos. Ocean. Technol.*, vol. 23, no. 12, pp. 1668–1681, Dec. 2006.

[14] E. Gorgucci and L. Baldini, "Attenuation and differential attenuation correction of C-band radar observations using a fully self-consistent methodology," *IEEE Geosci. Remote Sens. Lett.*, vol. 4, no. 2, pp. 326–330, Apr. 2007.

[15] J. Kalogiros, M. N. Anagnostou, E. N. Anagnostou, M. Montopoli, E. Picciotti, and F. S. Marzano, "Optimum estimation of rain microphysical parameters from X-band dual-polarization radar observables," *IEEE Trans. Geosci. Remote Sens.*, Jul. 2012, DOI: 10.1109/TGRS.2012.2211606.

[16] G. Scarchilli, E. Gorgucci, V. Chandrasekar, and T. Seliga, "Rainfall estimation using polarimetric techniques at C-band frequencies," *J. Appl. Meteorol.*, vol. 32, no. 6, pp. 1150–1160, Jun. 1993.

[17] P. Tabary, G. Vulpiani, J. J. Gourley, A. J. Illingworth, R. J. Thompson, and O. Bousquet, "Unusually high differential attenuation at C band: Results from a two-year analysis of the French Trappes polarimetric radar data," *J. Appl. Meteor.*, vol. 48, no. 10, pp. 2037–2053, 2009.

[18] J. Wurman, J. M. Straka, E. N. Rasmussen, M. Randall, and A. Zahrai, "Design and deployment of a portable, pencil-beam, pulsed, 3-cm Doppler radar," *J. Atmos. Ocean. Technol.*, vol. 14, no. 6, pp. 1502–1512, Dec. 1997.

[19] R. J. Doviak and D. S. Zrni, *Doppler Radar and Weather Observations*. San Diego, CA, USA: Academic, 1993, p. 562.

[20] A. Kruger and W. F. Krajewski, "Two-dimensional video disdrometer: A description," *J. Atmos. Ocean. Technol.*, vol. 19, no. 5, pp. 602–617, May 2002.

[21] J. Vivekanandan, G. Zhang, and E. Brandes, "Polarimetric radar estimates based on a constrained Gamma drop size distribution model," *J. Appl. Meteorol.*, vol. 43, no. 2, pp. 217–230, Feb. 2004.

[22] M. Schönhuber, W. L. Randeu, H. E. Urban, and J. P. V. Baptista, "Field measurements of raindrop orientation angles," in *Proc. AP Millennium Conf. Antennas Propag.*, Davos, Switzerland, 2000, pp. 1–40.

[23] G. J. Huang, V. N. Bringi, and M. Thurai, "Orientation angle distributions of drops after an 80-m fall using a 2D video disdrometer," *J. Atmos. Ocean. Technol.*, vol. 25, no. 9, pp. 1717–1723, Sep. 2008.

[24] K. V. Beard and C. Chuang, "A new model for the equilibrium shape of raindrops," *J. Atmos. Sci.*, vol. 44, pp. 1509–1524, Jun. 1987.

[25] M. I. Mishchenko, "Calculation of the amplitude matrix for a nonspherical particle in a fixed orientation," *Appl. Opt.*, vol. 39, no. 6, pp. 1026–1031, Feb. 2000.

[26] J. Hubbert and V. N. Bringi, "An iterative filtering technique for the analysis of copolar differential phase and dual-frequency polarimetric variables," *J. Atmos. Ocean. Technol.*, vol. 12, no. 3, pp. 643–648, 1995.

John Kalogiros received the B.Sc., M.Sc., and Ph.D. degrees from the Physics Department, University of Athens, Athens, Greece, in 1989, 1991, and 1997, respectively.

He was a Research Assistant with the Naval Postgraduate School, Monterey, CA, USA, from 2000 to 2002. He is currently an Assistant Researcher with the Institute of Environmental Research and Sustainable Development, National Observatory of Athens, Athens. His current research interests and accomplishments include polarimetric weather radar, acoustic sounder (sodar), and aircraft- and ground-based measurements of the atmospheric boundary layer.

Marios N. Anagnostou received the M.Eng. degree in avionics from York University, York, U.K., and the Ph.D. degree from the University of Connecticut, Storrs, CT, USA.

His current research interests include the implementation and validation of new advanced dual-polarization X-band algorithms on rainfall microphysics focused on mountainous and urban basins for high-resolution precipitation observation and estimation and flash-flood prediction.

Dr. Anagnostou was the recipient of the Group Achievement Award by NASA for the best group performance and the high quality of data collected in the CAMEX field experiment in 2002 and a European Union Marie Curie Intra-European Fellowship in 2009.

Emmanouil N. Anagnostou received the B.S. degree from the National Technical University, Athens, Greece, and the M.S. and Ph.D. degrees from the University of Iowa, Iowa City, IA, USA, all in civil and environmental engineering, in 1990, 1994, and 1997, respectively.

He is currently an Endowed Chair Professor with the Department of Civil and Environmental Engineering and Director of the Environmental Engineering Program, University of Connecticut, Storrs, CT, USA. His current research interests include the development of techniques for remote sensing of precipitation parameters from satellite and ground-based sensors and the integration of rainfall remote sensing products in hydrologic modeling for the prediction of floods and the study of regional water cycle.

Mario Montopoli received the Laurea degree in electronic engineering from the University of L'Aquila, L'Aquila, Italy, and the Ph.D. degree in radar meteorology from the University of Basilicata, Potenza, Italy, and the Sapienza University of Rome, Rome, Italy, through a joint program, in 2004 and 2008, respectively.

He has been with the Centro di Eccellenza per l'integrazione di Tecniche di Telerilevamento e Modellistica Numerica per la Previsione di Eventi Meteorologici Severi, University of L'Aquila, since 2005, where he is currently a Research Scientist on ground-based radar meteorology, with a special focus on C-band applications and processing techniques. Since 2006, he has also been a Research Assistant with the Department of Electrical and Information Engineering, University of L'Aquila.

Errico Picciotti received the Laurea degree (*cum laude*) in electrical engineering from the University of Ancona, Ancona, Italy, in 1993.

He was with the Science and Technology Park of Abruzzo, L'Aquila, Italy, in 1997, as a Radar Meteorologist. He was a Researcher with the Centro di Eccellenza per l'integrazione di Tecniche di Telerilevamento e Modellistica Numerica per la Previsione di Eventi Meteorologici Severi, University of L'Aquila, L'Aquila, in 2002, where he worked on radar systems and polarimetry. Since 2007, he has been with the CETEMPS Centre of Excellence, University of L'Aquila, where he is the Coordinator of the Radar Meteorology Division.

Frank Silvio Marzano (S'89–M'99–SM'03) received the Laurea degree (*cum laude*) in electronic engineering and the Ph.D. degree in applied electromagnetics from the Sapienza University of Rome, Rome, Italy, 1988 and 1993, respectively.

He was a Lecturer with the University of Perugia, Perugia, Italy After being with the Italian Space Agency. He joined the Department of Electrical Engineering in 1997 and co-founded the CETEMPS Centre of Excellence, University of L'Aquila, L'Aquila, Italy, in 2001. In 2005, he joined the Department of Electronic Engineering (now Dept. of Information Engineering), Sapienza University of Rome, where he currently teaches courses on antenna theory, electromagnetic propagation, and remote sensing. Since 2007, he has also been the Vice-Director of CETEMPS, University of L'Aquila. He is also involved in radio and optical propagation topics in relation to incoherent wave modeling, scintillation prediction, and rain fading analysis. His current research interests include passive and active remote sensing of the atmosphere, development of inversion methods, radiative transfer modeling, and radar meteorology.

Dr. Marzano has been acting as an Associated Editor of the IEEE GEOSCIENCE REMOTE SENSING LETTERS since 2004. He has also been an Associate Editor of the EGU's *Atmospheric Measurement Techniques* journal since 2011. He is a fellow of the Royal Meteorological Society, a Senior Member of the IEEE Geoscience and Remote Sensing Society, and a member of the American Meteorological Society. He was the recipient of the Young Scientist Award of XXIV General Assembly of URSI (Osaka, Japan) in 1993, the Best Paper Award from the EGU-Plinius Conferences in Nicosia, Cyprus and Savona, Italy, in 2008 and 2011, respectively, and the Best Oral Paper Award for a paper on propagation from the EuCAP Conference, Berlin, Germany, in 2009. He was the Italian National Delegate for the European COST actions n. 720, n. 280 and n. ES702, and n. IC0802 PropTNEO from 2001 to 2012. He has been the National Vice-Delegate for the COST Action Project IC1101 OpticWISE since 2011. He is a member of the Science team of the Global Precipitation Mission, the European Volcanic Ash Cloud Expert Group and a member of the EuMetSat Precipitation Science Advisory Group.